ELSEVIER

Journal of Molecular Catalysis A: Chemical 136 (1998) 91–104

JOURNAL OF MOLECULAR CATALYSIS A: CHEMICAL

New intermediate phases in formation at V–Mg–O catalyst

W. Oganowski, J. Hanuza *, L. Kępiński, W. Mišta, M. Mączka, A. Wyrostek, Z. Bukowski

W. Trzebiatowski Institute of Low Temperature and Structure Research, Polish Academy of Sciences, 50-950 Wrocław, Poland

Received 25 July 1997; accepted 16 January 1998

Abstract

The simulation of the active phase formation process at the V–Mg–O catalyst has been carried out using as a precursor, magnesium orthovanadate pretreated at different temperatures. Two intermediate phases of different structures were discovered and separated. X-ray diffraction, electron microscopy, chemical and thermogravimetric analyses and IR and Raman spectroscopies were used for the identification of both phases. The orthovanadate was found to be the final active product formed by the wet method of the synthesis. The catalytic activity of these new phases in the oxidative dehydrogenation of ethylbenzene to styrene was studied and compared to those of the supported V–Mg–O catalyst.

Keywords: V–Mg–O catalyst; Intermediate phases; Magnesium orthovanadate

1. Introduction

V–Mg–O systems are widely used as effective catalysts in the oxidative dehydrogenation of hydrocarbons [1–9]. Their catalytic properties are strongly influenced by the preparation procedure as a consequence of non-uniform distribution of vanadium on the support [3]. Contradictory conclusions have been drawn concerning the active components of these materials. Oganowski and Mišta [10] and Chaar et al. [11,12] attributed the active phase to the $Mg_3V_2O_8$ orthovanadate. On the other hand, Siew Hew Sam et al. suggested that α-$Mg_2V_2O_7$ pyrovanadate is the active component, but orthovanadate is responsible for the total oxidation [13]. The catalysts prepared by the impregnation contain this phase at much lower vanadia concentrations [3]. The samples prepared by the solid state reactions contain both phases in variable amounts since the pyrovanadate is the intermediate component [14]. Besides, the preparation procedure influences the morphology of the catalysts giving roughly amorphous phases which differ in the activities.

Our studies of the V_2O_5/MgO supported catalysts revealed that the active phase of this system is not detectable by the X-ray diffraction (XRD) method because of its high dispersion and low concentration. However, the nature of this phase can be characterized using indirect methods. In our opinion, the active phase of the

* Corresponding author. Fax: +48-71-441029; e-mail: hanuza@highscreen.int.pan.wroc.pl

1381-1169/98/$ - see front matter
PII: S1381-1169(98)00018-1

supported catalysts is formed by magnesium orthovanadate because this compound is thermodynamically stable in the systems containing excess of magnesium oxide. Therefore, the precursor of this compound was synthesized in the present study, in the same physical conditions and using the same procedure, as those reported previously for supported catalysts [15]. It means that the initial product was prepared in aqueous solutions using the molar ratio of the reagents corresponding to the $Mg_3V_2O_8$ stoichiometry. The 'precursor of the active phase', called phase I, was pretreated at different temperatures (up to 800°C) and all the products obtained in the intermediate temperatures were characterized by standard techniques. Since the V–Mg–O supported catalysts were used by us previously in the oxidative dehydrogenation of ethylbenzene to styrene which occurs at 520°C [16–18], also the product obtained by the heating of the precursor up to this temperature was included in our investigations. We suggest that the process of active phase formation in the supported V_2O_5/MgO catalysts can be simulated by the transformation of the phase I during the increasing of the temperature. The catalytic activity of these new phases was compared with that of the supported catalysts containing (by weight) 10.6% vanadium.

These studies confirm the earlier suggestions concerning the role of magnesium orthovanadate as the active phase of the supported V–Mg–O catalysts [10–12]. Moreover, the knowledge of the active phase formation process should be helpful in the synthesis of the modified and more efficient catalysts.

2. Experimental

2.1. Method of synthesis

The precursor of magnesium orthovanadate (phase I) was obtained from MgO (Reachim) and NH_4VO_3 (Merck) by mixing them in an aqueous solution in the molar ratio corresponding to the $Mg_3V_2O_8$ stoichiometry. The suspension was heated for 14 h at 80–90°C with intensive stirring, aged at room temperature (RT) for 200 h and then dried (with stirring) to a paste. This product was dried at 150–170°C, giving polycrystalline yellow powder. Phase I was heated for 30 min at 170–180, 200, 300, 520–550 and 800°C giving the products which were identified using several physicochemical techniques.

Some comparative studies have been performed in the present paper using the V_2O_5/MgO supported catalysts. These samples were prepared by the same method as described above for the precursor of magnesium orthovanadate. These catalysts were calcined at 520 and 800°C. They contain 10.6 wt.% of the vanadium.

2.2. Experimental techniques

The chemical composition of the products obtained was determined by atomic absorption spectroscopy (AAS) using a Perkin-Elmer 110 spectrophotometer. Phase identification was carried out by X-ray diffraction (XRD) technique using the powder method with a DRON-3 diffractometer (CoKα1, Fe filter). The collected data were processed by means of a POWDER PC program and the refinement of the unit cell parameters was performed with the LATCON program [19]. Thermal analysis (TG-DTA) was performed on a Linseis L-81 thermobalance over the temperature range 20–800°C. The reference material was Al_2O_3. Samples and reference were contained in Pt crucibles. The heating rate was 5°C/min and, in some cases, 10°C/min All curves were obtained in the static air atmosphere.

Electron micrographs were taken on a Philips CM 20 electron microscope using transmission and diffraction techniques. The voltage used was 200 kV. Powdered samples were deposited onto copper grids coated with perforated carbon films.

Fourier-transformed infrared (FTIR) transmission spectra were recorded in the 400–4000 cm^{-1} range on a Bruker IFS 88 spectrometer with 2 cm^{-1} resolution. The Raman scattering spectra (RS) were measured at 300 K in the 40–4000 cm^{-1} region. The 488 nm line of an Ar^{+} laser was used as the excitation source. A double monochromator DFS 24 of LOMO (Sant Petersburg) production and a cooled GaAs photomultiplier with a computer detection of 2 cm^{-1} resolution were used.

Diffuse reflectance (DR) spectra in the UV–visible region (200–850 nm) were collected with a Specord 500 Carl-Zeiss spectrophotometer equipped with a reflectance attachment. The resolution was 1 nm. The samples were pressed into a disk and as a reference $BaSO_4$ was used.

The catalyst test was performed in a flow V-type quartz reactor of 320 mm length and 20 mm inner diameter. Oxidative dehydrogenation of ethylbenzene to styrene was the test reaction. The molar ratio of the reagents was: ethylbenzene:oxygen:water = 1:2:20. The reaction temperature was 520°C and contact time 0.2 s. The 0.5 g sample was diluted with quartz to the 1:2 vol % and placed at the bottom of the reactor. The samples were pretreated at 520°C for 24 h in the flowing mixture of air and steam. The reaction products were analyzed by a GCHF 18.3 and a N-502 on-line chromatograph. The surface areas were determined by nitrogen absorption using a Sorptomatic 1900 equipment. The experimental details of the methods used have been described in our previous papers [16–18].

3. Results

3.1. X-ray diffraction

The chemical and AAS analyses indicate that the initial product prepared by the above described method (phase I) exhibits the same V/Mg ratio as appearing in magnesium orthovanadate. However, their XRD patterns significantly differ. Fig. 1 shows the XRD spectra of the phase I dried at 170, 200, 250, 320 and 500°C.

The XRD spectra of the as-synthesized and heated up to 250°C samples show the pattern of the three strong reflections and several weak lines. Our results indicate that such spectral contour is characteristic for the hydrated form of magnesium vanadate. The least square refinement of the obtained data allows to establish the lattice parameters as $a = 5.946$ Å and $c = 7.265$ Å of the hexagonal unit cell. The XRD data for

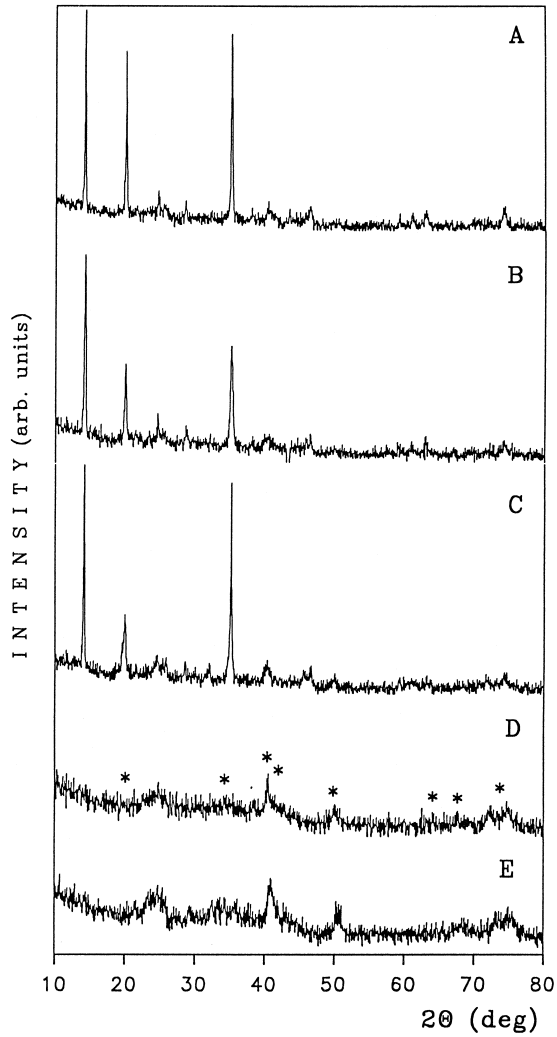

Fig. 1. X-ray diffraction spectra of the as-synthesized sample heated at 170°C (A), 200°C (B), 250°C (C), 320°C (D) and 500°C (E).

the phase I are listed in Table 1. It should be noted that these results were not found in the actual ICDD-PDF base of powders (International Center for Diffraction Data–Powder Diffraction File).

The XRD lines intensity of the phase I decreases when the temperature increases from 170 to 300°C. Simultaneously, the crystallinity of this phase is lowered up to 320°C where the phase I completely disappears (Fig. 1D). Above this point only the new amorphous phase exists (phase II), although its weak reflections are observed below this temperature. The XRD spectrum of the phase II is close to that of the tetragonally distorted spinel. The positions of the reflection lines for the cubic spinel with lattice parameter $a = 8.42$ Å [20] are marked in Fig. 1D.

Fig. 2A and B show the XRD spectra of the samples heated at 600 and 800°C, respectively. These spectra differ from those of the phases I and II. They contain exclusively the lines characteristic for $Mg_3V_2O_8$, being in good agreement with those observed by Siew Hew Sam et al. [13]. It means that above 600°C, the phase II transforms into the phase III, identified as magnesium orthovanadate. This high temperature phase is stable and has good crystallinity in the 600–800°C temperature range.

The XRD studies indicate that the two intermediate phases are formed during the temperature treatment of the $3MgO + V_2O_5$ system.

Table 1
XRD data of the hexagonal phase I

	hkl	*d* (Å)	$2\theta_{observed} - 2\theta_{calculated}$	I/I_1
1.	001	7.226	−0.001	95
2.	100	5.157	−0.027	80
3.	101	4.203	−0.007	12
4.	002	3.636	−0.028	8
5.	102	2.971	−0.032	100
6.	111	2.749	0.047	6
7.	003	2.422	0.000	5
8.	004	1.815	0.058	3
9.	203	1.765	−0.041	6
10.	212	1.715	0.026	12
11.	204	1.485	−0.023	14

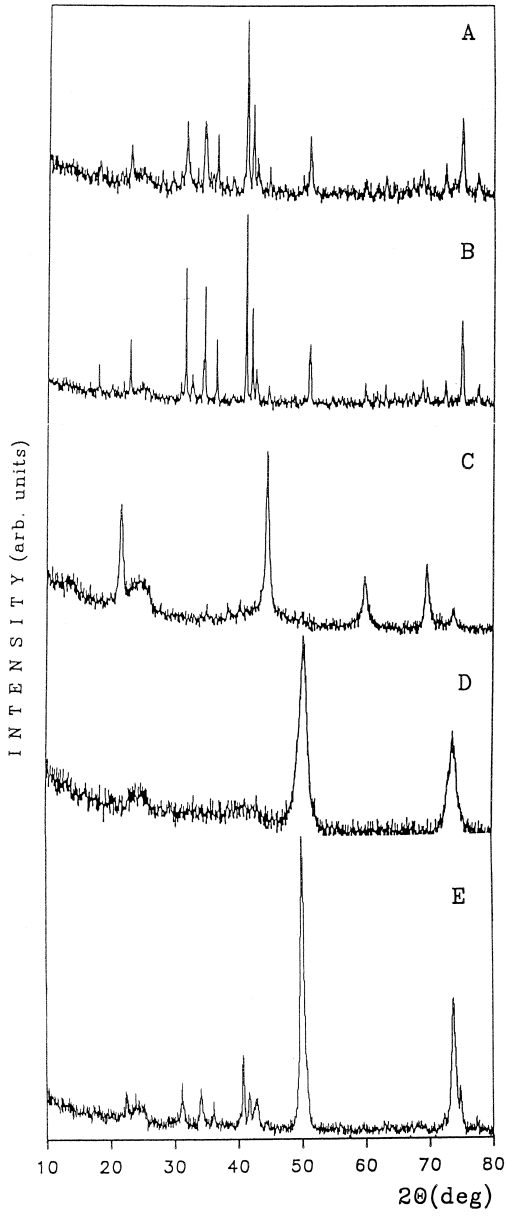

Fig. 2. XRD spectra of the samples heated at 600°C (A) and 800°C (B), as well as the V_2O_5/MgO catalyst calcined at 180°C (C) and 550°C (D) and 800°C (E).

Magnesium orthovanadate is the final product. Since the system studied simulates the active phase of the MgO/V_2O_5 supported catalyst, one can expect that the same three steps appear during the preparation of this catalyst with the low vanadium loading. The active phase of the

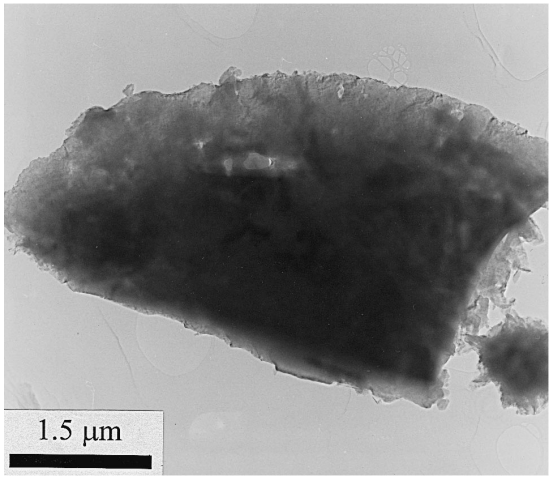

Fig. 3. Low magnification TEM micrograph of a plate-like crystal of the low-temperature phase I.

supported catalyst is highly dispersed and not detectable by the XRD method. This can be seen in Fig. 2C, D and E, where the XRD spectra of the supported MgO/V_2O_5 catalyst are shown. These samples were heated at 180, 550 and 800°C in the same conditions as the studied materials. The spectrum of the sample prepared at 180°C contains exclusively the lines corresponding to $Mg(OH)_2$. At 550°C this phase transforms into MgO (Fig. 2D) and its XRD spectrum does not indicate the existence of any other phase. The spectrum of the catalyst calcined at 800°C (Fig. 2E) exhibits the diffraction pattern characteristic for $Mg_3V_2O_8$ and MgO phases. It can be suggested that the phase I transforms above 300°C into phase II which is stable in the 300–600°C temperature range. Above 600°C the high-temperature phase III is formed. Since the catalytic reaction proceeds at 520°C the active phase of the supported catalyst is most likely formed by the dispersed phase II. In the catalysts calcined at 800°C the detectable by the XRD method (Fig. 2E) phase III appears.

3.2. Transmission electron microscope (TEM) and electron diffraction (ED) studies

The TEM micrographs and ED patterns of the phase I are shown in Figs. 3–5. This low-temperature phase forms a big plate-crystals with the size of several μm. Fig. 3 illustrates the example of the plate oriented perpendicularly to the electron beam. ED patterns of this crystal obtained for different settings of the goniometer are shown in Fig. 4. Taking into account strong reflections, it is possible to index the ED patterns in Fig. 4A and B as corresponding to [001] and [$\bar{1}$01] patterns of the hexagonal lattice with $a = 5.93$ Å and $c = 7.26$ Å. The crystals of the phase I were beam and vacuum sensitive and after an exposure in the electron beam their structure transformed from hexagonal to cubic. The ED pattern obtained for this

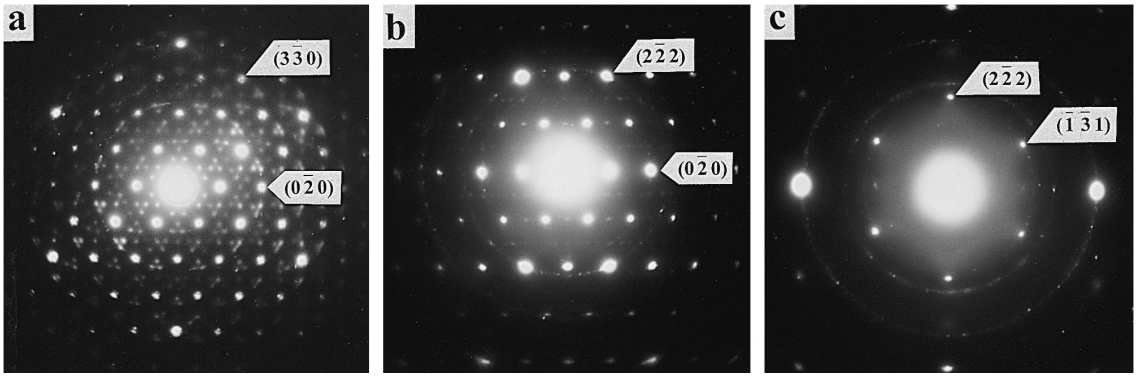

Fig. 4. Electron diffraction (ED) patterns of the crystal of phase I recorded at various orientations. [001] hexagonal pattern (a), [$\bar{1}$01] hexagonal pattern (b), and [$\bar{1}$12] cubic pattern (c). Note the change of the crystal structure from hexagonal to cubic and simultaneous partial destruction of the crystal lattice (occurrence of the continuous rings) during observation in TEM.

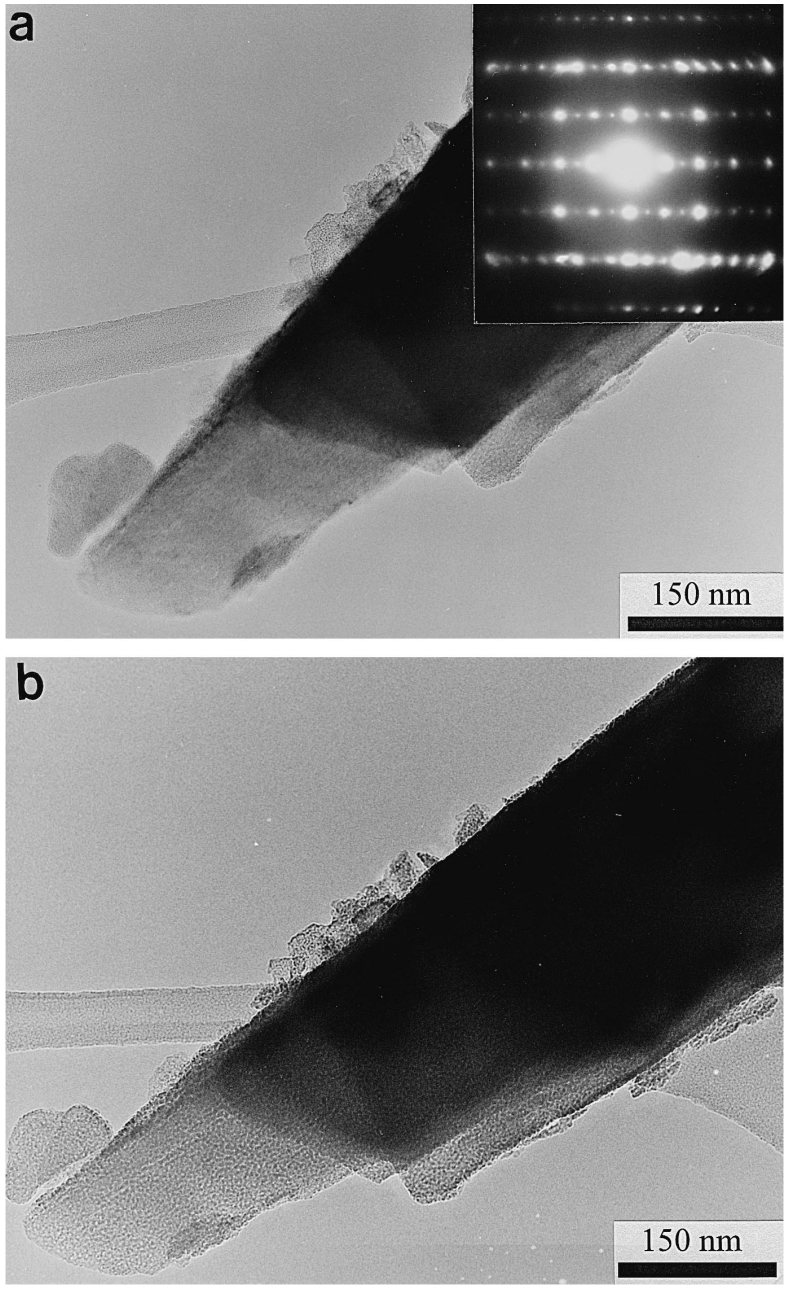

Fig. 5. TEM micrograph and ED pattern of the crystal of phase I in [010] orientation (a). The same crystal after prolonged (1 min) exposure to the electron beam (b). Note the destruction of the internal structure of the crystal in (b).

transformed phase is shown in Fig. 4C. The pattern corresponds to the cubic structure of the spinel type with lattice parameter close to 8.4 Å and oriented with the $[\bar{1}12]$ axis parallel to the electron beam.

Fig. 5A presents another plate crystal of the low-temperature phase. The ED pattern of this crystal (inset in Fig. 5A) has been indexed as the [010] pattern of the hexagonal lattice with the unit cell parameters the same as above.

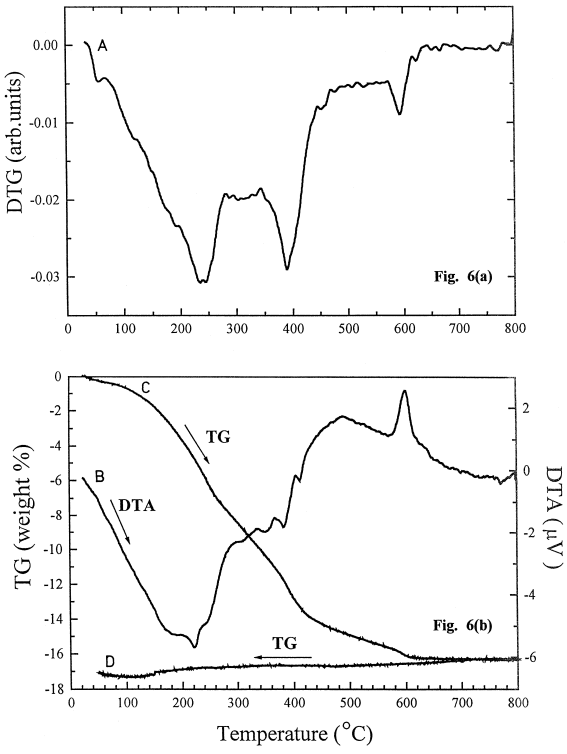

Fig. 6. DTG (a) and TG-DTA (b) curves of the as-synthesized sample heated at 170°C.

Fig. 5B shows the same crystal after 1 min exposure to the electron beam. It can also be seen from this micrograph that the electrons induce changes in the structure and destroy the structure of the phase I giving an amorphous product.

3.3. Thermogravimetric analyses

The TG-DTA and DTG curves for the as-synthesized sample are shown in Fig. 6. Fig. 7 presents the TG-DTA curves obtained for $Mg(OH)_2$. In Fig. 6 the endothermic broad peaks at ca. 220 and 400°C are observed. They are composed of several single processes at about 180, 220, 240°C, and 300, 340, 390 and 415°C, respectively. The weight loss in the former case is about 10.7% and for the latter 5.3%. In the 430–620°C range the progressive 2% weight loss is observed, being significantly slower. Overall mass loss in these processes is equal to 16%. It can be seen from the curves C and D that the process is not reversible in the 435–600°C range. The DTG curve (Fig. 6A) exhibits similar thermal behavior. Two strong and broad peaks at about 240 and 400°C are observed together with significantly weaker effects at 50 and 610°C. It is possible to assign the different thermal peaks to specific events appearing in the material studied. The events in the 100–

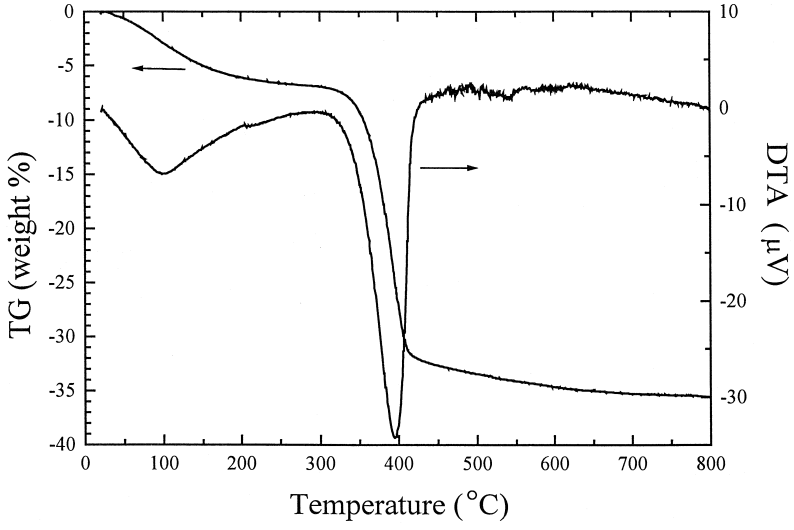

Fig. 7. TG-DTA curves of $Mg(OH)_2$ (Reachim).

350°C temperature range are attributed to the elimination of the two weakly bonded water molecules (12%). Strongly bonded water loss of another type appears in the 350–430°C temperature range. The exothermic effect at 600°C, visible in the DTA curve (Fig. 6B) is attributed to the phase III crystals formation effect. The nature of this change is analyzed below.

The thermogravimetric behavior of the phase I is compared to that of $Mg(OH)_2$ (Fig. 7). For this compound the two endothermic phenomena appear at about 100°C with the 6.8% and at 395°C with the 25.6% weight loss. The former corresponds to the removal of the adsorbed water and the latter to the $Mg(OH)_2 \rightarrow MgO + H_2O$ decomposition [13,14].

3.4. Infrared and raman studies

IR and Raman spectra of the as-synthesized phase heated at 170, 200, 300, 520 and 800°C are shown in Figs. 8 and 9. Several changes are

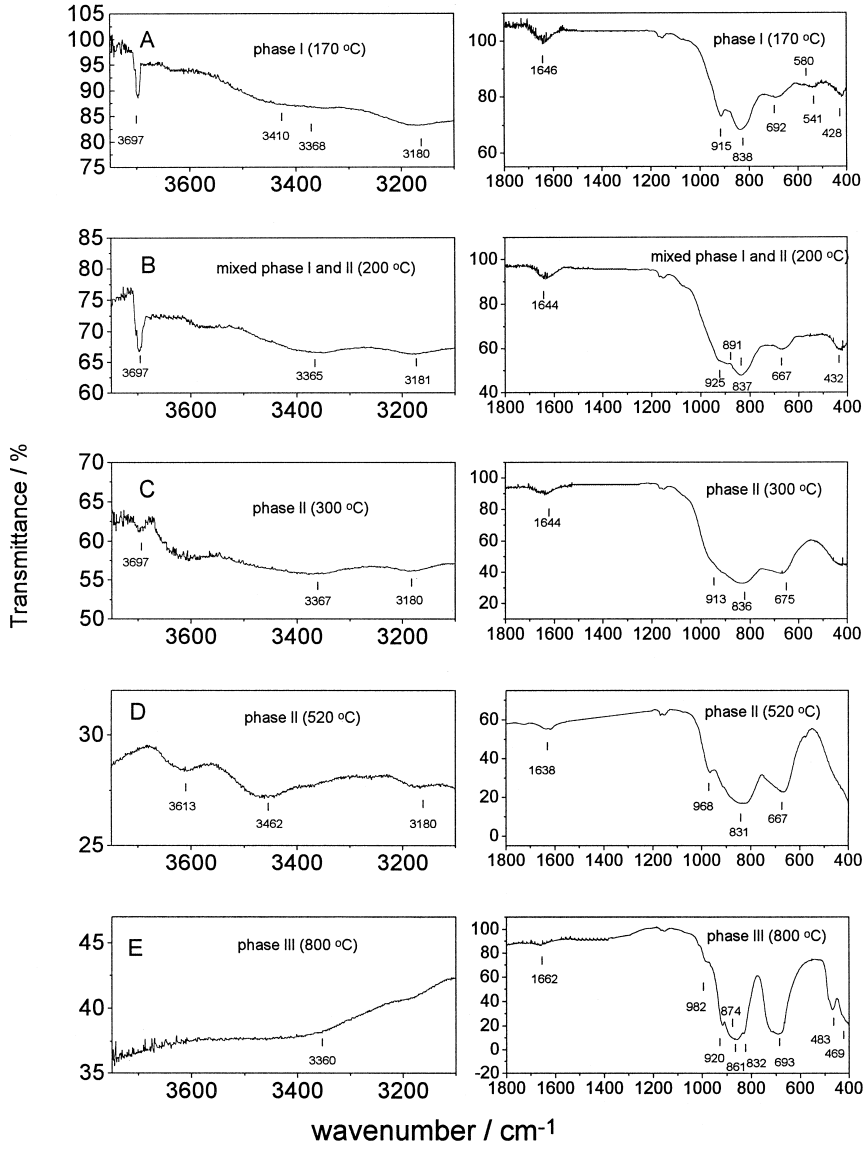

Fig. 8. IR spectra of the as-synthesized sample heated at 170°C (A), 200°C (B), 300°C (C), 520°C (D) and 800°C (E).

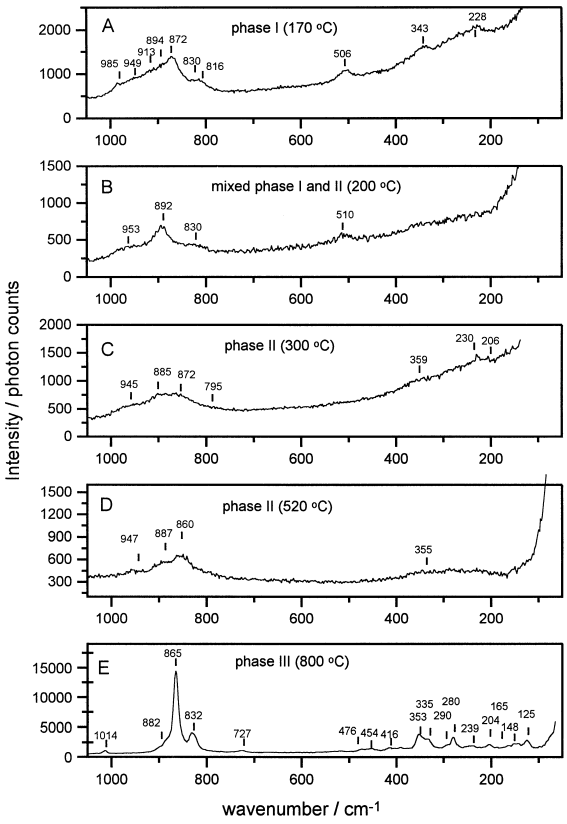

Fig. 9. Raman spectra of the as-synthesized sample heated at 170°C (A), 200°C (B), 300°C (C), 520°C (D) and 800°C (E).

observed in the vibrational spectra of these materials, depending on the thermal treatment. The IR spectrum of the sample heated at 170°C is composed of bands at 915, 838, 692, 541 and 428 cm^{-1} (Fig. 8A). Its Raman spectrum exhibits in this range several lined centered at 872, 820, 506, 343 and 228 cm^{-1} (Fig. 9A). Several IR bands are observed in the ν(OH) and δ(HOH) region at 3697, 3410, 3368, 3180 and 1646 cm^{-1}.

Some changes in the vibrational spectra are observed for the samples heated at 200 and 300°C,when phase I probably starts to transform into phase II (Fig. 8B, C and Fig. 9B, C). The IR band at 692 cm^{-1} shifts to 667 cm^{-1} for the sample heated at 200°C and 675 cm^{-1} for the 300°C sample. A similar trend can be observed in the Raman spectra, since the line at 872 cm^{-1} shifts at first to 892 cm^{-1} and then to 885 cm^{-1} with increasing temperature. Simultaneously, these bands broaden significantly. It should be noted that the band appearing in the IR spectrum of the phase I at 541 cm^{-1} disappears for the 200°C sample and this observed at 506 cm^{-1} in the Raman spectrum shifts to 510 cm^{-1} for the 200°C sample and completely disappears for the 300°C sample. The bands connected with the stretching and bending vibrations of the OH and H_2O units significantly decrease their intensities. The IR and Raman spectra of the sample heated at the reaction temperature i.e., at 520°C (Fig. 8D and Fig. 9D) are similar to those of the 300°C sample as far as the position and intensity of the bands are compared. However, the spectral contours are clearly narrower which makes the IR shoulder at 968 cm^{-1} clearly visible.

Further influence of the thermal treatment on the system studied can be seen from the IR and RS spectra of the sample heated at 800°C (Fig. 8D and Fig. 9D). The spectra measured for this

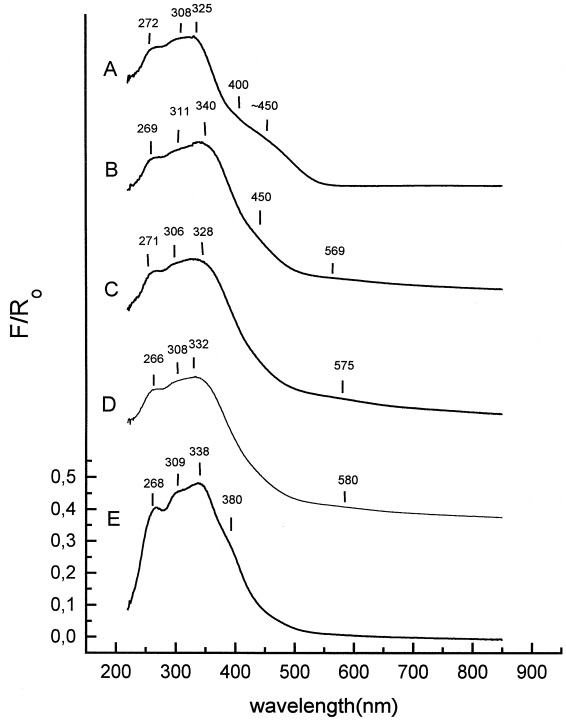

Fig. 10. DR spectra of the as-synthesized sample heated at 170°C (A), 200°C (B), 300°C (C), 520°C (D) and 800°C (E).

Table 2
Catalytic results for ethylbenzene oxidation over phases II and III and V–Mg–O supported catalysts

Catalysts	Calcination temperature (°C)	Surface area (m^2/g)	Conversion (wt.%)	Selectivity (%)	Yield (wt.%)		
					Styrene	$CO_2 + CO$	Benzene, toluene
Phase II	520	9.7	4.9	91.8	4.5	0.4	0.0
Phase III	800	4.8	0.1	100.0	0.1	0.0	0.0
V–Mg–O	520	182.0	68.0	85.3	58.0	8.9	1.1
V–Mg–O	800	32.0	51.8	91.5	47.4	4.2	0.2

phase are almost identical to those of the high-crystalline magnesium orthovanadate [11,13, 15,20].

3.5. Diffuse reflectance study

The DR spectra of the samples under study are shown in Fig. 10. The samples obtained by heating the as-synthesized material up to 200°C present high intensity charge transfer (CT) bands in the 260–500 nm region. The complex spectra exhibit two broad bands at about 270 and 330 nm and broad shoulders near 400 and 450 nm (Fig. 11A and B). The spectra of the samples heated at 300 and 520°C exhibit the above described doublet but the shoulder at 450 nm is only weakly marked for the former sample and completely disappears for the latter one. This means that in the range below 300°C the phase I exists and above this temperature the phase II is formed. This point on the temperature scale is very characteristic when the spectra above 500 nm are compared. For the samples heated at 300 and 520°C the clear shoulder at 580 nm is observed although it is barely visible for the sample obtained at 200°C. This band disappears for the phase III synthesized at 800°C. The DR spectrum of this sample consists of the multiplet at 260–340 nm and the additional shoulder at 380 nm.

3.6. Catalyst testing

The results of the catalyst test of the phase II and III as well as the supported V_2O_5/MgO catalyst are presented in Table 2. The ethylbenzene conversion, selectivity to styrene and yields of the oxidative dehydrogenation process and combustion reaction (CO_2, CO, benzene and toluene formation) are presented. It can be seen that the yield of the styrene for the phase II is very low (4.5%), but the phase III is virtually inactive in this process ($\sim 0.1\%$). Both phases deposited on the MgO and calcined at 520°C (Fig. 2D) and 800°C (Fig. 2E) form systems of high activity and selectivity. The yield of styrene for these samples is 58.0 and 47.4%, and selectivity to styrene 85.2 and 91.5%, respectively. The V–Mg–O catalyst calcined at 800°C exhibits insignificant (about 10%) lowering of styrene yield, what evidences its high stability. Generally speaking, the supported catalysts are much more active than the single phases II and III. The yield and conversion of these samples are one order of magnitude larger than those of phase II (4.5%). The phase II supported on MgO has the highest yield and conversion which suggests that the synergy effect exists between these phases.

4. Discussion

In the oxidative dehydrogenation of ethylbenzene to styrene, the V_2O_5/MgO catalysts prepared by the impregnation of the solid substrates in the aqueous solutions have been used previously [15]. This wet method was employed to the systems with low vanadium content (below 11% by weight). During the thermal treat-

ment, the characteristic chemical process takes place inside the active layer. The present studies show that the process of the active phase formation in the supported V–Mg–O catalysts can proceed by the intermediate stages. In the present paper we have simulated theses processes using precursor of $Mg_3V_2O_8$ orthovanadate (phase I) and heating it at different temperatures. The obtained products were identified using several physicochemical techniques. This approach appears to be reasonable since new intermediate phases have been discovered. Besides, the $Mg_3V_2O_8$ is the final product obtained from the phase I heated at 800°C. Similar product, (except MgO), is formed in supported V–Mg–O catalyst treated at identical conditions. It should be stressed, that their X-ray diffraction patterns are identical. Present studies indicate that the as-synthesized sample is composed of one single crystallographic phase of definite chemical composition. This compound contains 16.0 wt.% water. The Mg/V atomic ratio equals to 1.496. The DTA analysis (Fig. 6B) shows that the elimination of the two coordinated water molecules takes place up to 340°C and nearly overall deprotonation occurs with a loss of the water molecule formed probably by the combination of proton with the framework hydroxyl group. The integrated field under the DTG curve (Fig. 6A), corresponding to the former process, is twice as large as that of the latter one. The absorbed water constitutes about 0.7 wt.%.

The phase I could be identified on the basis of its chemical composition and IR, Raman and DR studies. The vibrational spectra of this compound differ from those reported for magnesium orthovanadate, pyrovanadate or metavanadate [11,13,15,20]. None of the bands characteristic for the pyrovanadate ($\sim$ 980, 820 cm^{-1}), orthovanadate ($\sim$ 860, 460 cm^{-1}) and metavanadate ($\sim$ 950, 880 and 740 cm^{-1}) appear in the spectrum of the phase I. Although the IR and RS multiplets in the 830–870 cm^{-1} range are typical for vanadium (V) oxy-compounds, their energetic positions are shifted as compared to the above mentioned compounds. The IR spectra of the phase I (Fig. 8A) consist of the bands at about 920, 838, 692 and 541 cm^{-1}. This contour resembles the spectrum of magnesium pyrovanadate [5,15,20] and therefore the bands at about 920 and 840 cm^{-1} could be assigned to the stretching vibrations of the terminal VO_4 group and those at about 690 and 540–580 cm^{-1} to the asymmetric and symmetric stretching motions of the V–O–V oxygen bridge. This similarity appears also when the RS spectra are compared [20]. The bands at 541 in the IR spectrum and 506 cm^{-1} in the Raman spectrum are particularly characteristic because they appear in the region typical for the symmetric stretching modes of the oxygen bond systems [21]. Several additional bands in the 3200–3700 cm^{-1} range correspond to the stretching vibrations of the water molecules and hydroxyl groups. The bands near 3700 cm^{-1} are characteristic for the ν(OH) vibrations and are in excellent agreement with the results obtained for $Mg(OH)_2$ lattice [22–25]. It should be noted that the spectra presented do not contain the band at 480 cm^{-1}, attributed to MgO [20]. It means that the sample studied was not contaminated with this phase.

The nature of the vanadium–oxygen species present in the phase I can also be determined from the DR spectra (Fig. 10). It is well known that the CT bands for the vanadium oxy-compounds are strongly influenced by the coordination and oxidation state [15,26–29]. The electron transitions for the V^{5+} ions in octahedral environment appear in the 350–500 nm region, whereas in tetrahedral coordination of the V^{5+} and V^{4+} are usually observed in the 500–850 nm region.

The spectral pattern observed in the present work for the phase I is located in the region significantly higher than expected for vanadium (V) in tetrahedral coordination (Fig. 10A and B). The bands at about 400 and 450 nm are very characteristic for the V^{5+} ions in distorted octahedral coordination. Thus, it can be concluded that the polymeric VO_6 units are present in the

molecular structure of the phase I. These results suggest that the general chemical formula of this phase could be written as $Mg_3(OH)_2$-$V_2O_7(H_2O)_2$. Its structure is composed of the distorted $VO_3(OH)(H_2O)$ octahedra joined by the V–O–V bridges. The XRD and TEM studies allow to describe this phase as hexagonal with the lattice parameters $a = 5.946$ and $c = 7.265$ Å. It forms yellow plates weakly crystallized and stable in air atmosphere up to 300°C.

The thermal treatment above 300°C leads to the phase transition with the formation of a new amorphous product. The XRD and TEM results suggest that the structure of the phase II is cubic (of the spinel type) with the lattice parameter $a \approx 8.4$ Å. This phase is strongly defected and probably isostructural to those formed from $Mg_3V_2O_8$ heated at 1000°C in the $N_2 + H_2$ atmosphere [30]. The changes in the IR and Raman spectra (Figs. 8 and 9) are consistent with the XRD and TEM studies. Because of the poor crystallinity, the full structural analysis of this phase could not be performed. However, its molecular structure my be deduced from the IR and DR studies. The structural transition from the phase I to the phase II leads to the IR shift of the band at 692 cm^{-1} to 667–675 cm^{-1} and disappearance of the band at 541 cm^{-1}. The simultaneous loss of two water molecules probably causes the formation of the polymeric structure, which consists of the VO_4 highly distorted tetrahedra joined by the

edges. The IR band at about 660 cm^{-1} is characteristic for the double oxygen bonded compounds [9,15]. The DR spectrum of the phase II (Fig. 10C and D) exhibits the typical multiplet observed for the orthovanadate ion which contains both the isolated and associated VO_4 tetrahedra [15,26,29]. In comparison to the phase I, the respective bands are significantly broadened due to the formation of the highly amorphous product.

At 300°C the elimination of two coordinated water molecules is finished and the deprotonation process occurs. This creates the best conditions for the V^{4+} centers formation, due to the defected structure of this phase. The highest intensity of the band at 580 nm, originating from the presence of the vanadium (IV) centers, is observed for the phase II prepared at about 300°C.

The thermal treatment of the phase I (above 600°C) causes its transition to the phase III. The exothermic effect observed for the DTA curves proves that the barrier of the activation energy was exceeded at this temperature and the recrystallization process had begun. The sharpness of the DTA peak suggests that this process was very fast. Similar thermic effects were observed for minerals with the layered structure [31]. They start from the initial, crystalline phase of mineral and proceed by the intermediate amorphous phase as a consequence of the dehydration and dehydroxylation process. In our case, magnesium orthovanadate $Mg_3V_2O_8$ with the good crystallinity is the final product of the thermal decomposition of the phase I. The results of the IR, Raman, XRD and DR studies of the phase III are in the good agreement with those reported for this compound [11, 13,15,22,32]. It can be noted that some differences appear in the IR and DR spectra of the phase III as compared to those of the standard orthovanadate [15,33]. The additional IR band at 982 cm^{-1} and shoulder at 380 nm in the DR spectrum can be observed. These effects suggest that the associated and strongly defected VO_4 tetrahedra are present in this phase.

Table 2 compares the selectivity and yields of the styrene for the phase II, III and the supported V_2O_5/MgO catalysts. Clear trends appear when these results are analyzed. The one order of magnitude higher activities are observed for the supported catalysts. Moreover, these values are significantly higher for the samples prepared at 520°C than those for the

samples synthesized at 800°C. These results coincide with the decreasing of the vanadium (IV) concentration in the high-temperature phase.

5. Conclusions

The aim of this paper was to simulate the transformations in the active phase of the supported V_2O_5/MgO catalysts using modeling composition of both oxides. This approach appear to be reasonable because new intermediate phases have been discovered and the final product obtained from the phase I (heated at 800°C) gives the same X-ray diffraction pattern as detected for the supported catalyst treated at the same temperature.

The comparative studies performed for the V–Mg–O supported catalyst (Fig. 2C and D) indicate that its active phase is not detected by means of the XRD method due to high dispersion and poor crystallinity. Our data obtained for the low-loading vanadium catalysts show that magnesium orthovanadate is the active phase for oxidative dehydrogenation of ethylbenzene to styrene [15]. This conclusion is in agreement with the results of Chaar et al. [12]. Present studies prove that in the thermal treatment during the calcination of the wet precursors several intermediate phases appear. The catalytic process occurs at 520°C. In this temperature the amorphous phase II (dispersed and very defected) forms the active layer and contains vanadium occupying non-isolated sites. These centers may be responsible for the selective oxidation.

During the preparation of the V–Mg–O catalyst by the wet method the hydrated form of alkali magnesium orthovanadate is probably formed inside the active layer as a product (phase I). The thermal activation transforms this phase into the phase II which is stable in the 300–600°C temperature range. Further increase of temperature yields the phase III, which is stable at the range 600–800°C. Phases II and III are composed of magnesium orthovanadate in the amorphous and crystalline states, respectively. Supported on the magnesium oxide both these phases are highly active in the oxidative dehydrogenation of ethylbenzene to styrene. The catalyst calcinated at 800°C exhibits high selectivity towards the formation of styrene. The activity of the phase II, which has the highest yield and conversion, is greatly improved by its supporting on MgO, suggesting that the synergy effect exists between these phases.

References

[1] M.C. Kung, H.H. Kung, J. Catal. 128 (1991) 287, and references therein.
[2] K.T. Nguyen, H.H. Kung, Ind. Eng. Chem. Res. 30 (1991) 352, and references therein.
[3] A. Corma, J.M. Lopez Nieto, N. Paredes, Appl. Catal. 104 (1993) 161, and references therein.
[4] P.M. Michalakos, M.C. Kung, I. Jahan, H.H. Kung, J. Catal. 140 (1993) 226, and references therein.
[5] X. Gao, P. Ruiz, Q. Xin, X. Guo, B. Delmon, J. Catal. 148 (56) (1994) and references therein.
[6] R. Juarez Lopez, N.S. Godjayeva, V. Cortes Corberan, J.L.G. Fierro, E.A. Mamedov, Appl. Catal. 124 (1995) 281, and references therein.
[7] W.S. Chang, J.Z. Chen, B.L. Yang, Appl. Catal. 124 (1995) 221, and references therein.
[8] E.A. Mamedov, V. Cortes Corberan, Appl. Catal. 127 (1995) 1, and references therein.
[9] W. Oganowski, J. Hanuza, H. Drulis, W. Mińta, L. Macalik, Appl. Catal. 136 (1996) 143, and references therein.
[10] W. Oganowski, W. Mińta, Bull. Pol. Acad. Sci., Chem. 32 (1984) 181.
[11] M.A. Chaar, D. Patel, M.C. Kung, H.H. Kung, J. Catal. 105 (1987) 483.
[12] M.A. Chaar, D. Patel, H.H. Kung, J. Catal. 109 (1988) 463.
[13] D. Siew Hew Sam, V. Soenen, J.C. Volta, J. Catal. 123 (1990) 417.
[14] G.M. Clark, R. Horley, J. Solid State Chem. 16 (1976) 429.
[15] J. Hanuza, B. Jeżowska-Trzebiatowska, W. Oganowski, J. Mol. Catal. 29 (1985) 109.
[16] W. Oganowski, Przemysł Chemiczny 73 (1994) 140.
[17] W. Oganowski, R. Klimkiewicz, Polish J. Chem. 67 (1993) 1787.
[18] W. Oganowski, J. Wrzyszcz, J. Chem. Stosow. 18 (1974) 67.
[19] W. Łasowska, K. Lewiński, J. Appl. Cryst. 27 (1994) 437.
[20] X. Gao, P. Ruiz, Q. Xin, X. Guo, B. Delmon, Catal. Lett. 23 (1994) 321.
[21] B. Jeżowska-Trzebiatowska, J. Hanuza, J. Mol. Struct. 19 (1973) 109.
[22] H.A. Benesi, J. Chem. Phys. 30 (1959) 852.

[23] F. Freund, in: V.C. Former (Ed.), The Infrared of Minerals, Mineralogical Society, 1974.
[24] R.T. Mara, G.B.B.M. Sutherland, J. Opt. Soc. Am. 43 (1953) 1100.
[25] M.R. Carrott, P. Carrott, M.B. de Carvalho, K.S.W. Sing, J. Chem. Soc. Faraday Trans. 89 (1993) 579.
[26] W. Hanke, R. Bienert, H.G. Jerschkewitz, Z. Anorg. Allg. Chem. 414 (1975) 109.
[27] G. Lischke, W. Hanke, H.G. Jerschkewitz, G. Öhlmann, J. Catal. 91 (1985) 54.
[28] J.G. Eon, R. Olier, J.C. Volta, J. Catal. 145 (1994) 318.
[29] J.M. Lopez Nieto, A. Dejoz, M.I. Vazquez, Appl. Catal. A. 132 (1995) 41.
[30] ASTM 19-778.
[31] L. Stoch, Metody Badań Minerałów i Skał (The Studies of the Minerals and Stones), Part IV, Thermal Methods, Wydawnictwo Geologiczne (Geological Publishing House), Warsaw, 1988.
[32] N. Krishnamachari, C. Calvo, Can. J. Chem. 49 (1971) 1630.
[33] J. Hanuza, W. Oganowski, B. Jeźowska-Trzebiatowska, Bull. Pol. Acad. Sci. Chem. 31 (1983) 153.